JACC: CASE REPORTS VOL. 30, NO. 40, 2025

IMAGING

BEYOND THE GUIDELINES

Machine Learning–Based CCTA-Guided Intensive Atheroprotective Strategy in a Middle-Aged INOCA Patient With Challenging Arterial Features

Alexander Kharlamov, MD,[a,b] Priscilla McElhinney, BSc,[c] Pieter Kitslaar, MSc,[d] Nicola Gaibazzi, MD,[e] Marco Guglielmo, MD,[f] Pim van der Harst, MD, PhD,[f] Avtandil Babunashvili, MD, PhD, DSc,[g,h] Alexei Sozykin, MD, PhD, DSc,[i] Damini Dey, PhD,[c] Gianluca Pontone, MD, PhD[j,k]

ABSTRACT

BACKGROUND Management of ischemia with nonobstructive coronary arteries (INOCA) remains insufficiently defined in current guidelines, particularly when complicated by symptomatic myocardial bridging, evolving nonobstructive atherosclerosis, and systemic inflammation. Such overlapping mechanisms create complex diagnostic and therapeutic challenges that require individualized care.

CASE SUMMARY A 39-year-old man with recurrent chest discomfort, left anterior descending myocardial bridging, and suspected microvascular dysfunction was found to have progressive high-risk atherosclerosis and elevated systemic inflammatory burden, despite the absence of obstructive coronary disease. Multimodal imaging—including coronary computed tomography angiography with machine learning (ML)-based ischemia risk scoring and pericoronary adipose tissue analysis—enabled precise characterization of both functional and structural risk. A tailored, intensive regimen targeting lipid lowering, myocardial unloading, and inflammation control led to regression of high-risk plaque features, reduction in pericoronary adipose tissue attenuation, normalization of inflammatory markers, and complete resolution of symptoms over 15 months.

WHY BEYOND THE GUIDELINES No established guideline recommendations address INOCA with concurrent symptomatic myocardial bridging, subclinical plaque progression, and residual inflammatory risk. A multimodal, off-label pharmacologic strategy was required to stabilize disease activity and restore functional status.

DISCUSSION This case underscores the utility of phenotype-specific, imaging-guided therapy in complex INOCA presentations. Integration of ML-enhanced coronary computed tomography angiography and individualized prevention enabled both anatomic regression and physiologic recovery in a high-risk but nonobstructive phenotype.

TAKE-HOME MESSAGES INOCA with symptomatic myocardial bridging and inflammation may require off-label, intensive therapy. ML-enhanced multimodal imaging facilitates dynamic risk stratification and tailored treatment adjustments. (JACC Case Rep. 2025;30:105907) © 2025 The Authors. Published by Elsevier on behalf of the American College of Cardiology Foundation. This is an open access article under the CC BY-NC-ND license (http://creativecommons.org/licenses/by-nc-nd/4.0/).

From the [a]De Haar Research Task Force (DHRF), The Hague, the Netherlands; [b]De Haar Research Foundation (DHRF) OÜ, Tallinn, Estonia; [c]Department of Biomedical Sciences, Biomedical Imaging Research Institute, Cedars Sinai Medical Center, Los Angeles, California, USA; [d]Medis Medical Imaging Systems BV, Leiden, the Netherlands; [e]Azienda Ospedaliero-Universitaria di Parma, Parma, Italy; [f]University Medical Center Utrecht, Utrecht, the Netherlands; [g]CELT Multidisciplinary Clinic (Center for Endosurgery and Lithotripsy), Moscow, Russia; [h]Department of Interventional Cardioangiology, Sechenov University, Moscow,

ISSN 2666-0849 https://doi.org/10.1016/j.jaccas.2025.105907

ABBREVIATIONS AND ACRONYMS

AI = artificial intelligence

CCTA = coronary computed tomography angiography

CT = computed tomography

FDG = fluorodeoxyglucose

FFR = fractional flow reserve

INOCA = ischemia with nonobstructive coronary arteries

LAD = left anterior descending artery

LDL-C = low-density lipoprotein cholesterol

MB = myocardial bridging

ML-IRS = machine learning ischemia risk score

PCAT = pericoronary adipose tissue

PET = positron emission tomography

Ischemia with nonobstructive coronary arteries (INOCA) encompasses a heterogeneous clinical spectrum defined by objective evidence of myocardial ischemia in the absence of obstructive epicardial coronary artery disease. Contemporary guidelines from the European Society of Cardiology, American Heart Association, and Coronary Vasomotor Disorders International Study Group recommend 3 diagnostic criteria: presence of ischemic symptoms or imaging-based perfusion abnormalities; angiographic evidence of <50% stenosis with preserved fractional flow reserve (FFR) (>0.80) or instantaneous wave-free ratio (iFR) (>0.89); and exclusion of nonischemic causes such as myocarditis or hypertrophic cardiomyopathy. INOCA mechanisms may include coronary microvascular dysfunction, vasospasm, or structural anomalies such as myocardial bridging (MB), which often coexist and evolve dynamically, necessitating multimodal diagnostic strategies.

Yet, current clinical guidelines provide limited direction for managing symptomatic MB within the INOCA framework, particularly in the setting of coexisting systemic inflammation, high-risk but nonobstructive plaque morphology, and borderline hemodynamic parameters. In such scenarios, the need for personalized, imaging-guided management becomes paramount—especially when invasive physiology and static luminal measurements fail to capture the evolving ischemic potential.

This report presents a complex case of INOCA in a middle-aged patient with high-risk nonobstructive plaques, systemic inflammatory comorbidities, and a previously asymptomatic myocardial bridge that became functionally significant. We highlight the integration of coronary computed tomography angiography (CCTA), perfusion imaging, invasive physiology, and artificial intelligence (AI)-based plaque analysis in guiding intensive, phenotype-driven prevention. The case underscores the necessity of multimodal diagnostics and tailored treatment in bridging the current gap between guideline frameworks and real-world INOCA complexity.

TAKE-HOME MESSAGES

- INOCA with symptomatic myocardial bridging and high-risk nonobstructive plaques may require a personalized, imaging-guided strategy that addresses both dynamic ischemia and subclinical atherosclerosis.
- Integration of CCTA-derived plaque features, PCAT inflammation, and ML-based risk scoring can guide intensive prevention beyond conventional revascularization thresholds.

CASE SUMMARY

A 39-year-old male executive, enrolled in the REALITY Advanced trial (ClinicalTrials.gov identifier: NCT02440646), presented with exertional palpitations, recurrent chest discomfort, and presyncope. He reported no prior cardiac history. Risk profile included hypertension, dyslipidemia, prediabetes, former smoking, and secondary hypogonadism (Supplemental Tables 1 to 4). Several chronic comorbidities—idiopathic pulmonary fibrosis, early nonalcoholic steatohepatitis, chronic atrophic gastritis, duodenitis, and mild nephropathy—suggested systemic low-grade inflammation (**Figure 1**). Genetic testing (Supplemental Table 1) revealed a cluster of proinflammatory, thrombogenic, and vasoreactive polymorphisms—including IL6 (interleukin-6), IL1β (interleukin-1 beta), TNF-α (tumor necrosis factor-alpha), TGF-β1 (transforming growth factor-beta 1), NOS3 (endothelial nitric oxide synthase), MMP1 (matrix metallopeptidase 1), and FGB (fibrinogen beta chain)—reflecting enhanced susceptibility to endothelial dysfunction, coronary spasm, and acute atherothrombosis, despite the absence of a family history of premature coronary artery disease.

CCTA revealed a long myocardial bridge (42.2 mm, with 66% systolic compression and 18.9-mm

Russia; [i]Department of X-ray Endovascular Diagnostics and Treatment, Scientific and Clinical Center No. 2, Petrovsky National Research Centre of Surgery, Moscow, Russia; [j]Department of Perioperative Cardiology and Cardiovascular Imaging, Centro Cardiologico Monzino IRCCS, Milan, Italy; and the [k]Department of Biomedical, Surgical and Dental Sciences, University of Milan, Milan, Italy.

The authors attest they are in compliance with human studies committees and animal welfare regulations of the authors' institutions and Food and Drug Administration guidelines, including patient consent where appropriate. For more information, visit the Author Center.

Manuscript received August 20, 2025; revised manuscript received September 15, 2025, accepted September 22, 2025.

VISUAL SUMMARY **AI-Guided Inflammatory Risk Dynamics and Therapeutic Response in a Patient With INOCA and Myocardial Bridging**

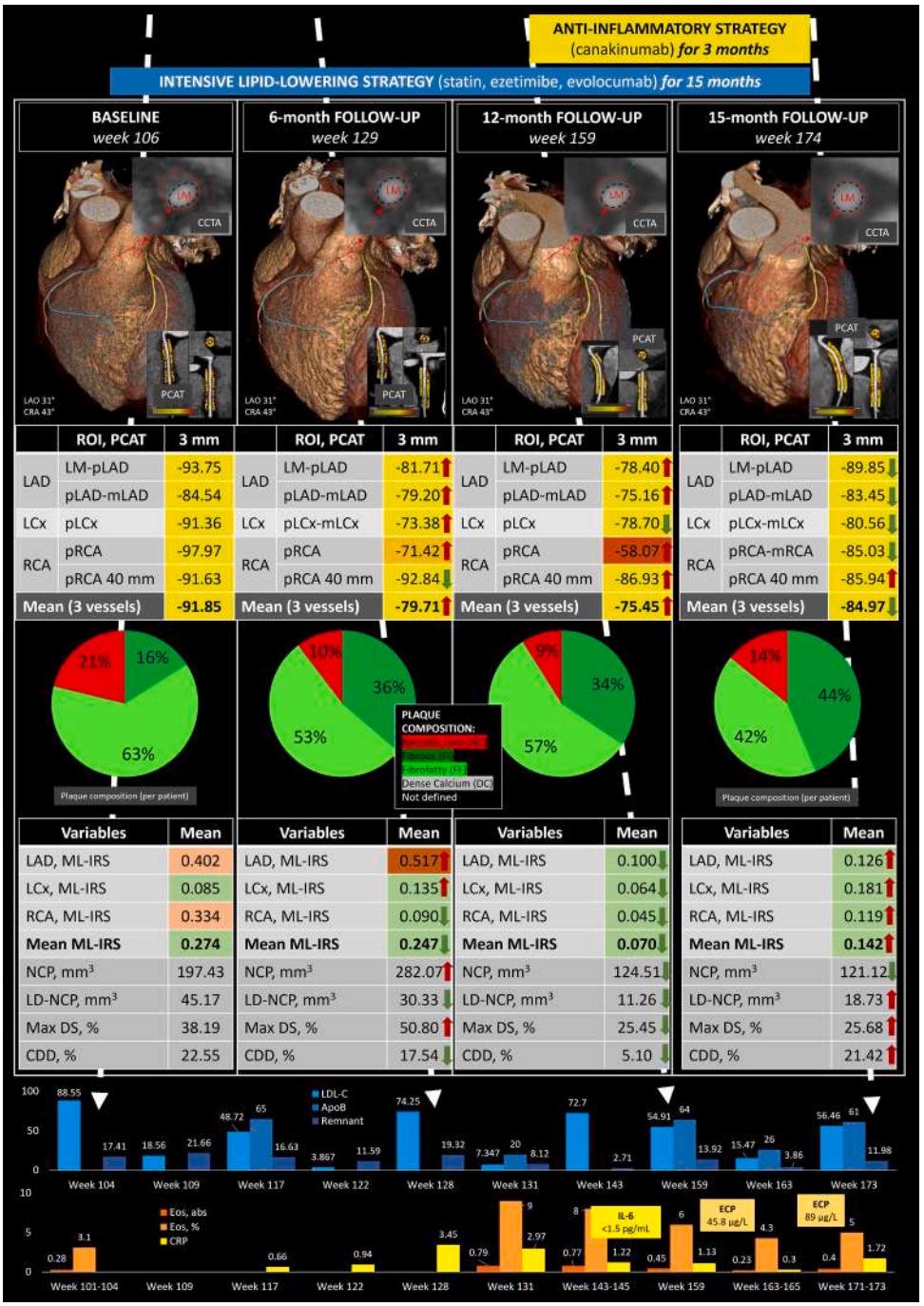

Serial CCTA with AI-based analysis was used to monitor coronary inflammation and ischemic risk in a patient with INOCA and myocardial bridging. Pericoronary adipose tissue (PCAT) attenuation in the proximal LAD increased from −97.97 to −58.07 HU despite intensive lipid-lowering therapy, reflecting persistent vascular inflammation. Introduction of targeted anti-inflammatory treatment resulted in a marked PCAT reduction to −98.85 HU. The machine learning ischemia risk score (ML-IRS) progressively decreased from a baseline mean of 0.274 (maximum: 0.402) to 0.247 (maximum: 0.517) during lipid-lowering therapy alone. After anti-inflammatory intervention, the ML-IRS dropped further to 0.070 after 12 months, with a corresponding value of 0.142 at 15 months, indicating a sustained reduction in lesion-related ischemic potential. The lower panel displays biochemical improvements over the same period: LDL-C declined from 138.8 to 7.3 mg/dL, remnant cholesterol from 24.8 to 0.07 mg/dL, ApoB from 94 to 20 mg/dL, and hsCRP from 3.45 to <0.3 mg/L. These findings underscore the additive value of inflammation-targeted therapy in patients with residual ischemic risk despite optimal lipid control. AI = artificial intelligence; ApoB = apolipoprotein B; CCTA = coronary computed tomography angiography; hsCRP = high-sensitivity C-reactive protein; INOCA = ischemia with nonobstructive coronary arteries; LAD = left anterior coronary artery; LCx = left circumflex artery; LDL-C = low-density lipoprotein cholesterol; RCA = right coronary artery; ROI = region of interest.

FIGURE 1 Systemic Determinants and Multiorgan Manifestations of Chronic Inflammation in an INOCA Patient With Diffuse Atherosclerosis

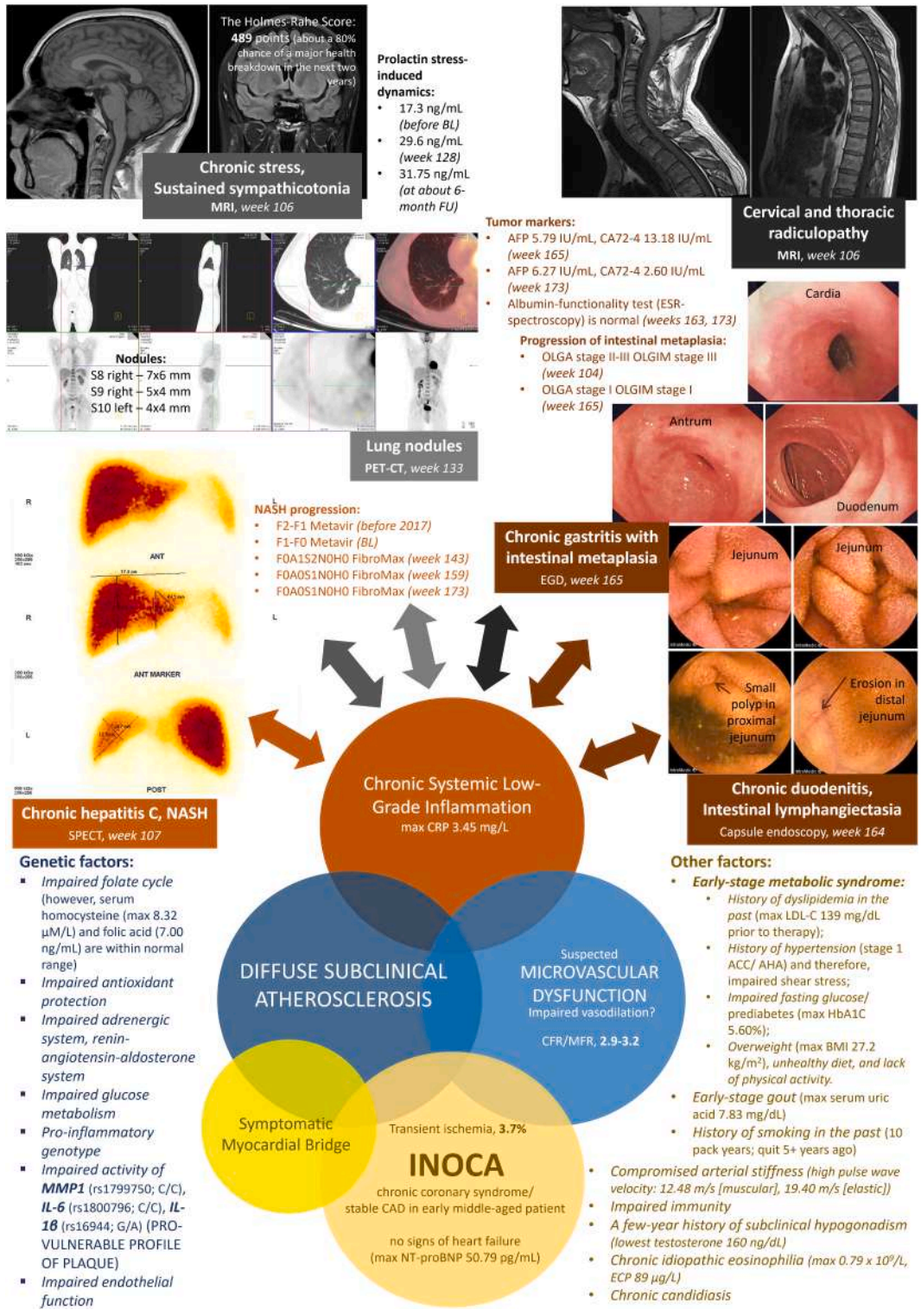

Continued on the next page

myocardial depth) over the mid left anterior descending artery (LAD), consistent with a prior silent anomaly (**Figures 2 and 3**). However, the emergence of symptoms raised concern for an acquired hemodynamic component. Adjacent to the bridge, proximal LAD lesions progressed to 40% to 41% stenosis, with lipid-rich necrotic cores in the left main and proximal right coronary artery segments (**Figure 4**). AI-assisted plaque analysis identified high-risk features, elevated pericoronary adipose tissue attenuation, and a machine learning ischemia risk score (ML-IRS) of >0.4 (Supplemental Figures 1 to 4). FFR on computed tomography (CT) was preserved, except in the distal left circumflex artery (0.83), and invasive iFR in the bridged segment was borderline (0.87), without evidence of in-bridge atheroma (**Figure 5**).

Multimodal functional imaging was undertaken to resolve diagnostic ambiguity and assess ischemic burden: SPECT (single-photon emission computed tomography) showed reversible anterolateral defects, cardiac magnetic resonance revealed segmental strain abnormalities, and ^{13}N-ammonia positron emission tomography (PET) quantified a transient ischemic burden of 3.7% (**Figure 3**). Discordant localization between modalities suggested concomitant microvascular dysfunction. ^{18}F-fluorodeoxyglucose (FDG) PET/CT excluded myocardial inflammation.

The diagnosis of INOCA was established based on 1) objective evidence of ischemia, 2) absence of flow-limiting epicardial stenoses, and 3) exclusion of alternative diagnoses. The evolving clinical picture—conversion of previously asymptomatic MB into a symptom-generating substrate—was attributed to localized plaque progression, microvascular dysfunction, and systemic inflammation.

To address both myocardial stress and inflammatory atherogenesis, a multidisciplinary heart team initiated intensive preventive therapy, aiming for regression of vulnerable plaques and restoration of coronary flow reserve (**Figure 6**). The strategy combined high-intensity lipid-lowering (atorvastatin, ezetimibe, evolocumab), anti-inflammatory (canakinumab, later replaced with colchicine) therapy, neurohormonal modulation (sacubitril/valsartan, carvedilol), metabolic protection (dapagliflozin), and testosterone supplementation.

This comprehensive regimen was justified not solely by anatomical findings, but by the integration of multimodal functional imaging and systemic inflammatory risk. CCTA served both as a diagnostic and longitudinal monitoring tool, confirming significant plaque regression and pericoronary adipose tissue (PCAT) improvement. Regression of high-risk plaque features (**Figure 6**, Supplemental Figures 3 to 5) and ML-IRS decline paralleled the patient's return to a symptom-free state. Despite limited prognostic data for such approaches in INOCA, the observed clinical and imaging response supported its use in this specific context.

WHY BEYOND THE GUIDELINES

This case exemplifies a clinical scenario not addressed by existing guideline-directed algorithms: A previously asymptomatic myocardial bridge that became symptomatic in the setting of progressive nonobstructive but high-risk atherosclerosis, systemic inflammation, and discordant ischemia across

FIGURE 1 Continued

This figure illustrates the multiorgan contributors to chronic systemic low-grade inflammation in a middle-aged patient with INOCA, integrating findings from imaging, genetic, gastrointestinal, endocrine, metabolic, and rheumatologic evaluations. (Center Panel) A conceptual model links 4 interacting disease domains—diffuse subclinical atherosclerosis, microvascular dysfunction, symptomatic myocardial bridging, and chronic inflammation—culminating in INOCA with transient ischemia (3.7%) and preserved NT-proBNP levels (≤50.79 pg/mL). (Left and Bottom Panels) Chronic inflammation is supported by elevated hsCRP (peak: 3.45 mg/L), chronic hepatitis C (eliminated, but with residual NASH), and impaired antioxidant, glucose, and adrenergic regulation. Genetic variants affecting IL-6, IL-1β, and MMP1 suggest a proinflammatory and plaque-vulnerable genotype. (Right Panels) Gastrointestinal contributions include OLGA stage III intestinal metaplasia (regressing to stage I), capsule endoscopy–verified intestinal lymphangiectasia, and jejunal erosions (weeks 164-165), along with *H. pylori*–negative chronic gastritis. (Top Right) MRI at baseline (week 106) revealed cervical/thoracic radiculopathy and central stress markers. The Holmes-Rahe score reached 489 points, indicating >80% risk of major health deterioration. Prolactin elevation confirmed sustained sympathicotonia. (Bottom Right) Additional factors: These include impaired endothelial function, early-stage metabolic syndrome (HbA1c: 5.6%, prior LDL-C: 139 mg/dL), prior smoking, chronic candidiasis, and signs of arterial stiffness. Collectively, this figure supports the hypothesis that chronic systemic inflammation—driven by multifactorial and multiorgan pathology—plays a central role in INOCA pathophysiology, beyond focal coronary anatomy. HbA1c = hemoglobin A1c; hsCRP = high-sensitivity C-reactive protein; INOCA = ischemia with nonobstructive coronary arteries; LDL-C = low-density lipoprotein cholesterol; MRI = magnetic resonance imaging; NASH = nonalcoholic steatohepatitis; NT-proBNP = N-terminal pro-B-type natriuretic peptide.

FIGURE 2 **Anatomical and Functional Characterization of a Long Myocardial Bridge in the LAD With Associated Ischemia**

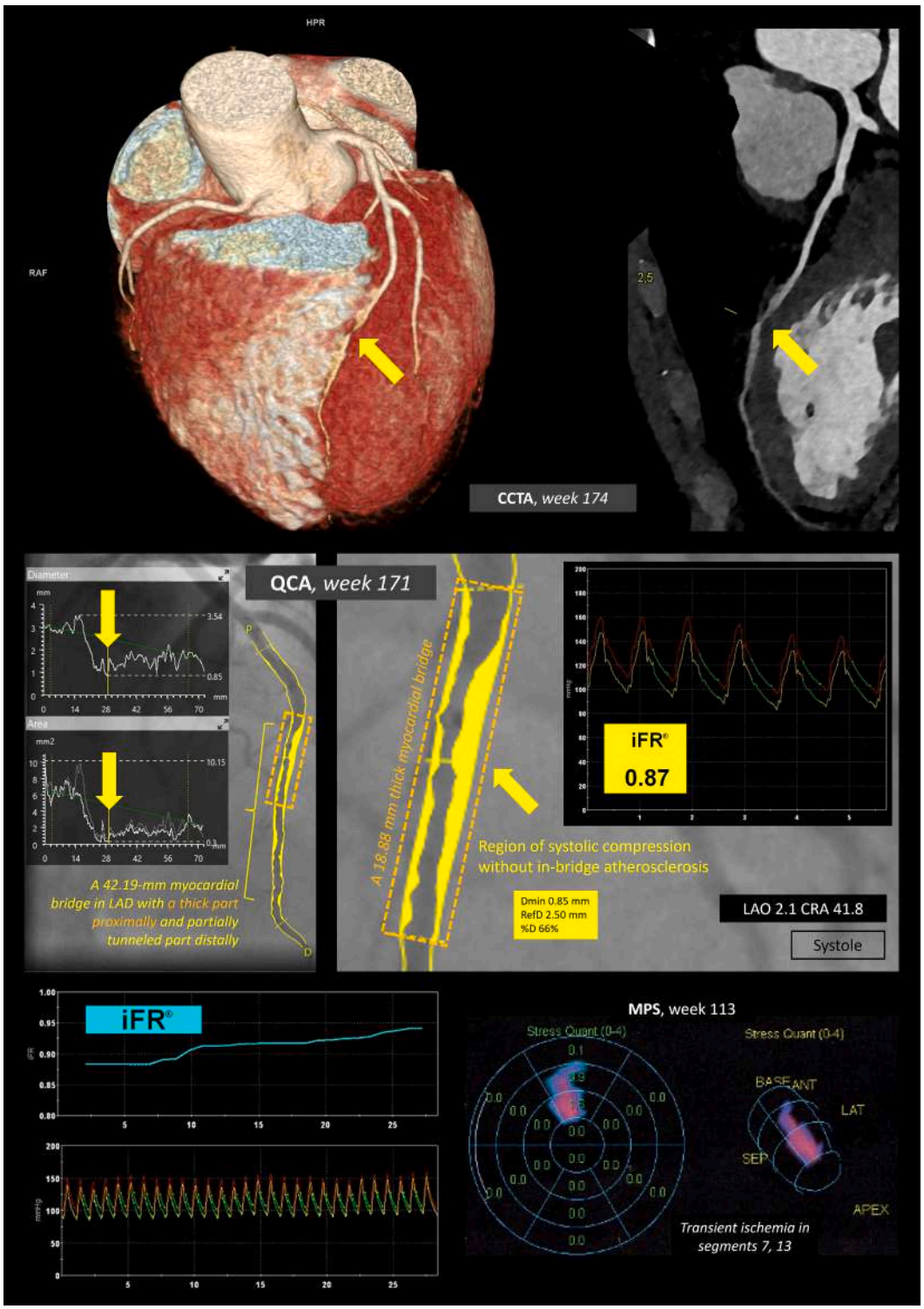

Continued on the next page

multiple imaging modalities. Although the measured iFR (0.87) was above the conventional ischemic threshold, it likely underestimated the dynamic flow-limiting impact of the bridge; the concomitant presence of lipid-rich necrotic cores and elevated PCAT attenuation proximal to the MB supported inflammation-driven vulnerability. Standard management would not typically prompt the use of advanced imaging, invasive physiology, or intensive lipid-lowering and anti-inflammatory therapy in the absence of obstructive stenosis. However, in this patient, multimodal characterization revealed an evolving ischemic phenotype requiring a personalized approach focused on plaque stabilization, myocardial unloading, and control of residual inflammatory risk. This strategy—guided by integrative interpretation rather than fixed thresholds—falls outside current recommendations and underscores the importance of individualized, imaging-informed management in complex INOCA presentations.

CASE OUTCOME AND FOLLOW-UP

The implementation of an intensive, phenotype-specific therapeutic regimen led to a marked and sustained clinical benefit. Within 3 months, the patient experienced full resolution of exertional chest discomfort and presyncopal episodes, with restored exercise capacity and improved functional status. This symptomatic relief—sustained throughout follow-up—translated into a tangible improvement in quality of life, which had been significantly impaired prior to treatment initiation.

Multimodal imaging confirmed the concordant physiological response. Follow-up ^{13}N-ammonia PET and gated myocardial perfusion scintigraphy demonstrated resolution of previously observed perfusion deficits, including those associated with the bridge-dependent LAD territory (**Figure 3**, Supplemental Figures 2 to 9). Cardiac magnetic resonance imaging showed normalization of regional strain parameters, while ^{18}F-FDG PET/CT excluded myocardial inflammation.

Serial CCTA served as the cornerstone of anatomical and inflammatory plaque monitoring. Quantitative analysis revealed significant regression of high-risk plaque components in multiple vascular territories (**Table 1**, Supplemental Tables 5 to 10). Total plaque volume decreased by 36.9%, lipid-rich necrotic core by 75.1%, and necrotic core fraction by 72.7%, as documented in Supplemental Tables 8 and 9 and visualized in Supplemental Figure 8. AI-based CCTA further demonstrated a substantial decline in PCAT attenuation (from −58.1 to −98.9 HU), indicating reduced perivascular inflammation in the proximal LAD. This finding paralleled the dramatic drop in the ML-IRS (from 0.402 to 0.070) and aligns with prior studies linking elevated PCAT with local coronary inflammation and plaque instability.

Biochemical response mirrored the imaging findings (Supplemental Tables 2 to 4): Low-density lipoprotein cholesterol (LDL-C) fell from 138.8 to 7.3 mg/dL, remnant cholesterol from 24.8 to 0.07 mg/dL, apolipoprotein B from 94 to 20 mg/dL, and high-sensitivity C-reactive protein from 3.45 to <0.3 mg/L (**Figure 5**, Supplemental Table 2). This dual-targeted approach—aimed at both lipid burden and residual inflammatory risk—was justified by the patient's baseline immuno-inflammatory profile, including chronic comorbidities and proinflammatory genetic polymorphisms (**Figures 1 and 4**). The initial use of interleukin-1β blockade with

FIGURE 2 Continued

This figure summarizes the multimodal assessment of a long myocardial bridge in the LAD integrating CCTA, invasive QCA, intravascular physiology, and MPS. (Top Panels) Three-dimensionally rendered and multiplanar CCTA (week 174) demonstrates a 42.19-mm myocardial bridge in the mid-LAD, with a thick proximal segment and partially tunneled distal portion (yellow arrows). (Middle Panels) QCA (week 171) shows systolic compression of the bridged segment, with a minimal luminal diameter of 0.85 mm and a diameter reduction of 66%. The myocardium surrounding the LAD bridge was 18.88-mm thick. The compressed segment lacked in-bridge atherosclerotic plaque. Functional assessment: iFR measured 0.87 within the bridge, indicating borderline hemodynamic significance; iFR tracing shows a systolic pressure drop without clear diastolic impairment, consistent with dynamic extrinsic compression rather than fixed epicardial stenosis. (Bottom Right) MPS at week 113 revealed a small but reproducible area of reversible ischemia in segments 7 and 13 (anterior/apical), corresponding to the bridged LAD territory. Together, these findings support the clinical significance of a long myocardial bridge in the context of INOCA, where transient ischemia is mediated by dynamic systolic compression in the absence of obstructive atherosclerosis. CCTA = coronary computed tomography angiography; iFR = instantaneous wave-free ratio; INOCA = ischemia with nonobstructive coronary arteries; LAD = left anterior descending artery; MPS = myocardial perfusion scintigraphy; QCA = quantitative coronary angiography.

FIGURE 3 **Multimodal Functional Assessment of Ischemia in INOCA With Myocardial Bridging and Diffuse Atherosclerosis**

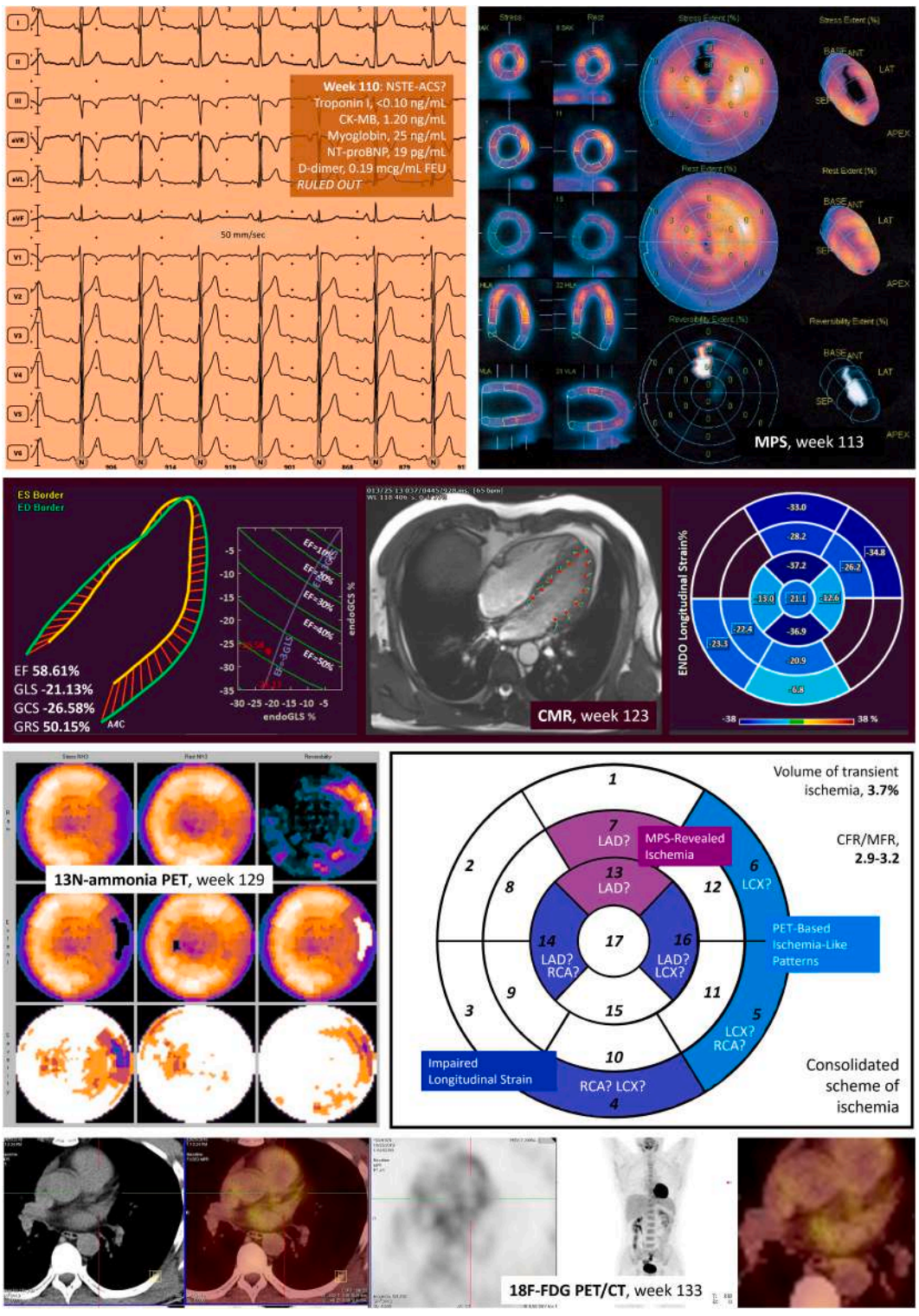

Continued on the next page

canakinumab, followed by colchicine, was guided by the persistence of subclinical inflammation despite lipid control and was central to long-term stabilization.

Beyond biochemical and anatomical outcomes, the therapeutic goal of myocardial unloading was also achieved. Neurohormonal modulation and optimized metabolic therapy contributed to reduced wall stress and restoration of myocardial perfusion, as evidenced by the normalization of ischemic indices and improvement in myocardial strain parameters. The combination of structural regression and functional recovery confirmed the efficacy of a strategy designed not merely to prevent events, but to reverse the dynamic ischemic substrate of INOCA in a patient with overlapping mechanisms of supply-demand mismatch.

Despite good medication adherence, the patient's lifestyle—marked by occupational stress, irregular diet, and physical inactivity—was recognized as a persistent risk factor. In light of the high-risk baseline anatomy, especially in the proximal LAD and left main segments, continued CCTA surveillance was advised every 12 to 24 months, or sooner if symptoms recurred. Such monitoring was considered essential given the chronic inflammatory background and the progressive nature of nonobstructive plaque evolution, as emphasized in recent INOCA and chronic coronary syndrome paradigms.

Throughout follow-up, we continuously assessed the benefit-risk balance with structured safety monitoring, and all potential risks were discussed with the patient a priori. Therapeutic intent prioritized plaque regression—beyond very low LDL-C or mere stabilization—by intensifying lipid lowering and coupling it with targeted control of residual inflammatory risk in the context of chronic low-grade inflammation. Neurohormonal modulation with sacubitril/valsartan in combination with beta-blockade was selected to counter maladaptive renin-angiotensin-aldosterone system/sympathetic activation and unload the myocardium, a mechanism expected to mitigate ischemia in the MB/INOCA phenotype, while also serving as proactive prevention of heart failure progression; short courses of calcium-channel antagonists were layered to temper dynamic compression when needed. Potential adverse effects discussed a priori and specifically monitored included myalgia/myopathy, transaminitis and injection-site reactions (statin/ezetimibe/PCSK9i); infection risk, cytopenias and gastrointestinal intolerance with myotoxicity (canakinumab/colchicine); hypotension, renal dysfunction, hyperkalemia and angioedema (sacubitril/valsartan); bradycardia and fatigue (carvedilol); genitourinary infections, volume depletion and euglycemic ketoacidosis (dapagliflozin); bleeding (rivaroxaban) and headache/flushing (dipyridamole); and polycythemia/edema with a prothrombotic signal (testosterone). A structured safety plan (vital signs and symptom check at each visit; periodic creatine kinase, aspartate transaminase/alanine transaminase, creatinine/estimated glomerular filtration rate, potassium/sodium, hematocrit/hemoglobin, and urinalysis when indicated) showed no clinically significant adverse events or treatment-limiting

FIGURE 3 Continued

This figure presents the integrated diagnostic work-up of suspected myocardial ischemia using serial multimodal noninvasive testing in a patient with INOCA. (Top Left) At week 110, the patient experienced presyncope, prompting evaluation for NSTE-ACS. Electrocardiography showed no ischemic ST-T changes, and biomarkers (troponin I: <0.10 ng/mL; CK-MB: 1.20 ng/mL; NT-proBNP: 19.2 pg/mL) were within normal limits. ACS was ruled out. (Top Right) Myocardial perfusion scintigraphy (week 113) demonstrated a reversible perfusion defect suggestive of stress-induced ischemia localized to segment 13 (mid-anterior wall). (Middle Panels) Cardiac magnetic resonance (week 123) revealed preserved ejection fraction (58.6%) with impaired global longitudinal strain (−21.1%), global circumferential strain (−26.6%), and focal reduction in endocardial longitudinal strain in the apical and anterior segments. (Lower Left) Dynamic ^{13}N-ammonia PET (week 129) showed areas of reversible perfusion impairment overlapping with the findings on myocardial perfusion scintigraphy, with a calculated transient ischemic volume of 3.7% and preserved coronary flow reserve (2.9-3.2). (Lower Center) Consolidated ischemia map combining anatomical segments and modality-specific findings localized ischemic signatures to the LAD and possibly LCx territories. (Lower Right) ^{18}F-FDG PET/CT (week 133) revealed no active myocardial inflammation or infiltration. These results support a diagnosis of stress-induced ischemia without obstructive CAD, attributed to a combination of myocardial bridging, microvascular dysfunction, and inflammatory activity. FDG = fluorodeoxyglucose; CAD = coronary artery disease; CK-MB = creatine kinase-MB; CT = computed tomography; INOCA = ischemia with nonobstructive coronary arteries; LAD = left anterior descending artery; LCx = left circumflex artery; NSTE-ACS = non ST-segment elevation acute coronary syndrome; NT-proBNP = N-terminal pro-B-type natriuretic peptide; PET = positron emission tomography.

FIGURE 4 **Invasive Coronary Angiography With Quantitative Coronary Analysis at Week 171**

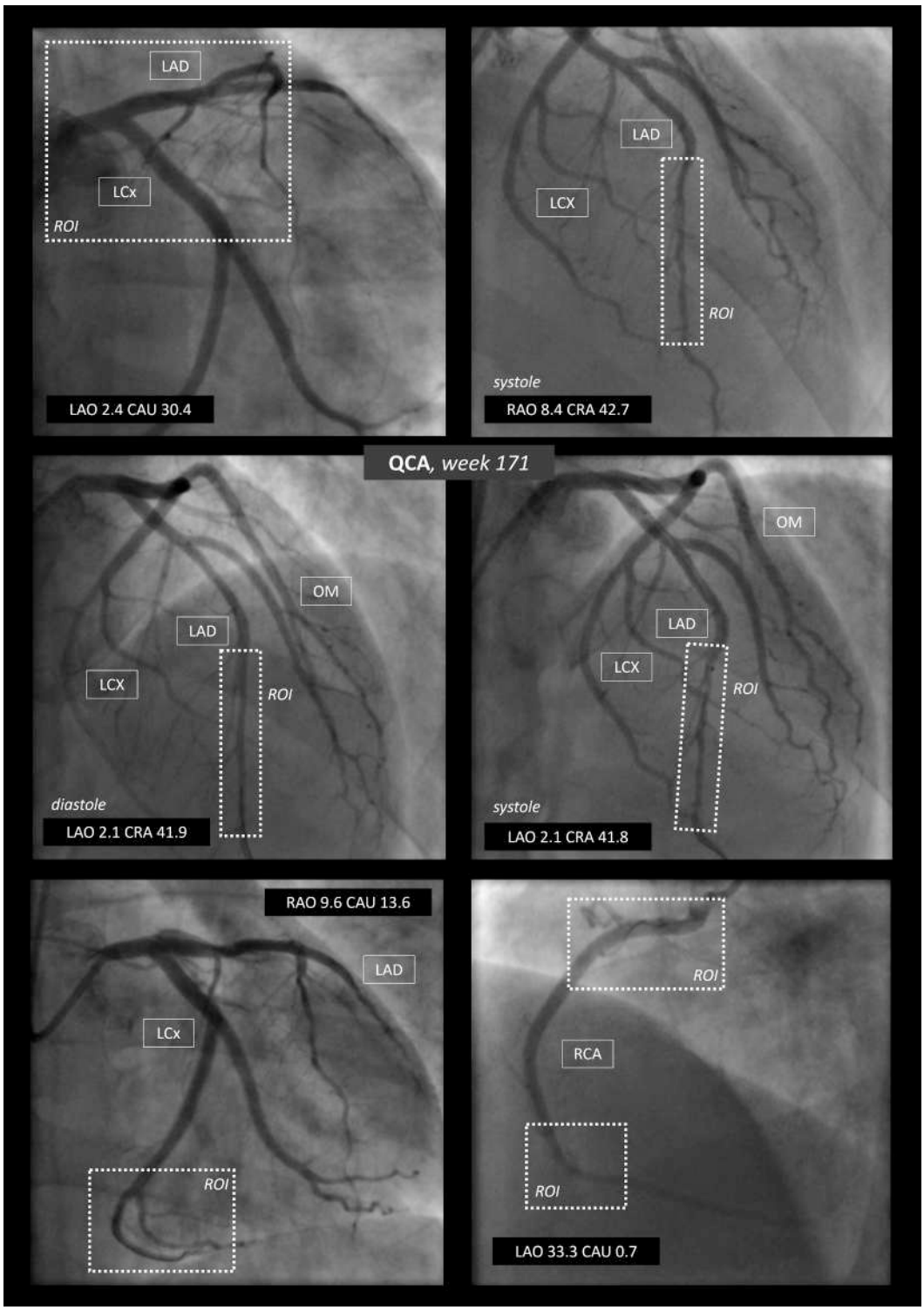

Continued on the next page

intolerance over follow-up. Taken together with the magnitude of clinical and imaging responses, these findings support the feasibility and favorable net benefit of a monitored, phenotype-guided off-label strategy aimed at plaque regression, control of residual inflammatory risk, and myocardial unloading in complex INOCA, while warranting vigilant surveillance and a low threshold for dose adjustment or withdrawal at the first signal of harm.

DISCUSSION

This case underscores the complexity of INOCA as a clinical and mechanistic entity, wherein ischemia arises from the interplay of functional, structural, and inflammatory contributors rather than fixed luminal obstruction. In this patient, symptomatic MB, progressive nonobstructive atherosclerosis, and systemic low-grade inflammation formed a pathogenic triad that could not be captured by anatomy or single-modality testing alone.

Although MB is often dismissed as a benign anatomical variant, accumulating evidence implicates long, deep, and dynamically compressed bridges in effort-related INOCA.[1,2] The present case illustrates a phenotype wherein MB became symptomatic only after progression of high-risk atherosclerosis proximal to the bridged segment—suggesting that fixed and dynamic lesions can synergize to lower ischemic thresholds. The borderline iFR (0.87) further demonstrates the limited sensitivity of resting indices in this context, particularly when diastolic compression and microvascular dysfunction coexist.[3]

The presence of nonobstructive, lipid-rich, and inflamed plaques introduced a critical second dimension to this case. CCTA-derived features such as low-attenuation plaque, positive remodeling, and elevated PCAT attenuation are well-established markers of vulnerability, even in the absence of ≥50% stenosis.[4,5] In this patient, AI-based ML-IRS provided a composite ischemia index that captured lesion complexity beyond diameter stenosis, consistent with the PARADIGM and CRISP-CT findings.[5,6] Importantly, the management strategy was not limited to identifying high-risk plaque but extended to addressing its biology through intensive lipid lowering. Early and sustained reduction of LDL-C has been shown to slow atherosclerotic progression and delay the onset of cardiovascular events; cumulative exposure to LDL-C across the life course is a key determinant of lifetime risk, and earlier, longer periods of LDL-C lowering provide greater benefits than later intervention. This principle—"the lower, the earlier, the longer"—has been summarized in the European Atherosclerosis Society 2017 consensus statement.[7] Thus, the integration of advanced imaging-based risk stratification with an intensive preventive approach targeting plaque regression can be viewed as a form of proactive cardiovascular protection.

The systemic inflammatory milieu added a third pathophysiologic axis, shaping both coronary microvascular function and plaque behavior. The patient's chronic multisystem conditions and elevated high-sensitivity C-reactive protein reflected a residual inflammatory risk phenotype, increasingly recognized as a therapeutic target in both primary

FIGURE 4 Continued

This figure displays selected projections from invasive coronary angiography with QCA performed at 33-month follow-up (week 171) in a patient with INOCA and previously documented high-risk nonobstructive coronary lesions. (Top and Middle Panels) Angiographic frames demonstrate the LAD, LCx, and OM in multiple projections including LAO/RAO and cranial/caudal views. ROI boxes outline the proximal and mid-LAD segments, which were previously identified on coronary CTA as harboring diffuse, lipid-rich, nonobstructive plaques and a myocardial bridge. Systolic and diastolic frames show no dynamic luminal compression or significant flow-limiting stenosis. (Bottom Left) The left coronary system, including the LCx and LAD, appears free of hemodynamically significant obstruction, with preserved distal flow. ROI indicates the territory of the previously noted perfusion mismatch on PET and CMR. (Bottom Right) The RCA is visualized in a steep LAO/caudal projection. ROI boxes highlight the proximal and mid-RCA segments previously shown to contain high-risk plaques with elevated ML-IRS and PCAT inflammation markers, yet no obstructive disease is apparent on angiography. Overall, QCA confirmed the absence of obstructive coronary artery disease despite prior evidence of ischemia and high-risk plaque features. This supports a diagnosis of INOCA with contributions from microvascular dysfunction and myocardial bridging rather than epicardial stenosis. CAU = caudal; CMR = cardiac magnetic resonance; CRA = cranial; CTA =computed tomography angiography; INOCA = ischemia with nonobstructive coronary arteries; LAD = left anterior descending artery; LAO = left anterior oblique; LCx = left circumflex artery; ML-IRS = machine learning ischemia risk score; OM = obtuse marginal artery; PCAT = pericoronary adipose tissue; PET = positron emission tomography; QCA = quantitative coronary analysis; RAO = right anterior oblique; RCA = right coronary artery; ROI = region of interest.

FIGURE 5 Serial AI-Based Modeling of Coronary Hemodynamics, Inflammation, and Plaque Stabilization Over 12 Months

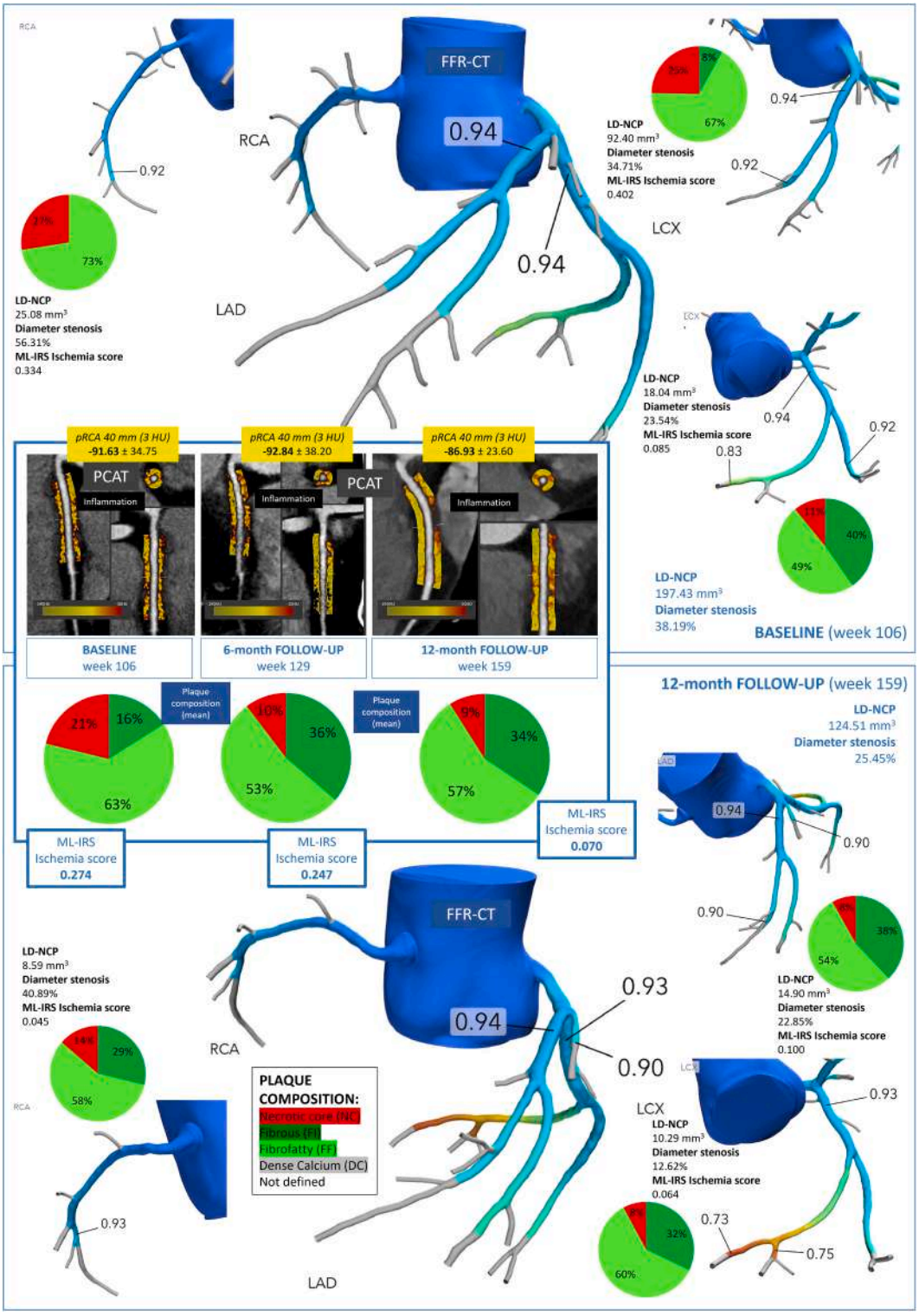

Continued on the next page

and secondary prevention.[8] Trials such as CANTOS, COLCOT, and LoDoCo2 have demonstrated that suppressing low-grade inflammation—independent of lipid levels—can reduce cardiovascular events. Although off-label, the use of canakinumab and colchicine in this case was mechanistically justified by persistent inflammatory activation, proinflammatory polymorphisms (Supplemental Figures 1 and 6), and imaging markers such as elevated PCAT attenuation.

The rationale for a multimodal, intensive preventive strategy was thus anchored in several converging observations: 1) symptoms arose in a previously asymptomatic myocardial bridge, suggesting a dynamic shift in pathophysiology; 2) CCTA showed progression of high-risk nonobstructive plaques; 3) functional imaging identified heterogeneous ischemia consistent with MB, atherosclerosis, and microvascular dysfunction; and 4) inflammatory biomarkers and imaging supported an active systemic and vascular inflammatory state. Importantly, this approach aligns with the "treat-to-target" philosophy explored in the WARRIOR trial, which demonstrated improved symptom control and quality of life in women with INOCA undergoing intensive risk factor modification—even in the absence of revascularization.[9]

The success of this individualized regimen—evidenced by imaging-confirmed plaque regression, ischemia resolution, and improved quality of life—highlights the clinical value of phenotype-driven, imaging-guided care in patients falling outside traditional revascularization paradigms. Although randomized trials in this population remain scarce, expert consensus from both European (European Society of Cardiology/European Association of Percutaneous Cardiovascular Interventions) and American (American Heart Association/American College of Cardiology) societies emphasizes the importance of intensive preventive strategies in patients with ischemia and nonobstructive coronary disease.[10] Despite differences, both sets of guidelines stop short of endorsing multimodal, off-label approaches such as the one described here, which should therefore be understood as an individualized, phenotype-guided intervention rather than a standard recommendation. Digital tools such as ML-IRS, plaque quantification, and PCAT assessment may eventually form the backbone of precision cardiovascular prevention in this high-risk but undertreated population.[11-14]

Beyond the demonstration of plaque regression, the applied approach also aimed at systemic anti-inflammatory control and partial reversal of metabolic syndrome, thereby targeting not only vascular but also systemic drivers of residual risk. By unloading the myocardium and modulating neurohormonal activation, the regimen was intended to proactively prevent the transition to overt heart failure, a critical endpoint in the continuum of chronic coronary disease. Taken together, the convergence of lipid lowering, inflammation suppression, and metabolic optimization provides a multidimensional preventive effect: reducing the

FIGURE 5 Continued

This figure displays 3D reconstructions of serial coronary CTA-based computational models integrating FFR_{CT}, PCAT attenuation, machine learning ischemia risk scores (ML-IRS), and plaque composition metrics across baseline (week 106), 6-month (week 129), and 12-month (week 159) follow-up. (Top and Middle Panels) FFR_{CT} values remained within the nonobstructive range (≥0.83) across major coronary segments, but ischemic potential varied by plaque morphology and vessel segment. At baseline, ML-IRS values were elevated (eg, 0.402 in the LAD, 0.334 in the RCA) and necrotic core (NC) content was high (eg, 27% in RCA, 25% in LAD), despite modest diameter stenosis. Over 12 months, the ML-IRS dropped markedly (to 0.070), while NC content decreased and fibrous/fibrofatty components increased, indicating compositional plaque stabilization. (Center Panels) Serial PCAT assessment in the proximal RCA segment showed decreasing inflammation (from −91.6 to −86.9 HU) after intensive lipid-lowering and anti-inflammatory therapy. Mean plaque composition shifted from 21% NC/63% fibrous (week 106) to 9% NC/57% fibrous (week 159), aligning with ML-IRS decline. (Bottom Panel) At 12 months, ML-IRS scores were universally low (0.045-0.100) across all vessels, and low-density noncalcified plaque (LD-NCP) volumes decreased (eg, from 197.4 to 124.5 mm^3 in the LAD). Despite stable anatomical stenoses, functional and inflammatory improvements were evident, highlighting the utility of longitudinal AI-driven imaging biomarkers for noninvasive monitoring. This comprehensive modeling underscores the feasibility of precision-guided, noninvasive secondary prevention in INOCA by visualizing dynamic improvements in coronary physiology and plaque vulnerability. 3D = three-dimensional; AI = artificial intelligence; CTA = computed tomography angiography; FFR_{CT} = fractional flow reserve derived from computed tomography; INOCA = ischemia with nonobstructive coronary arteries; LAD = left anterior descending artery; LCx = left circumflex artery; PCAT = pericoronary adipose tissue; RCA = right coronary artery.

FIGURE 6 **Longitudinal Trajectories of Biomarkers and Therapeutic Interventions in a Patient With INOCA**

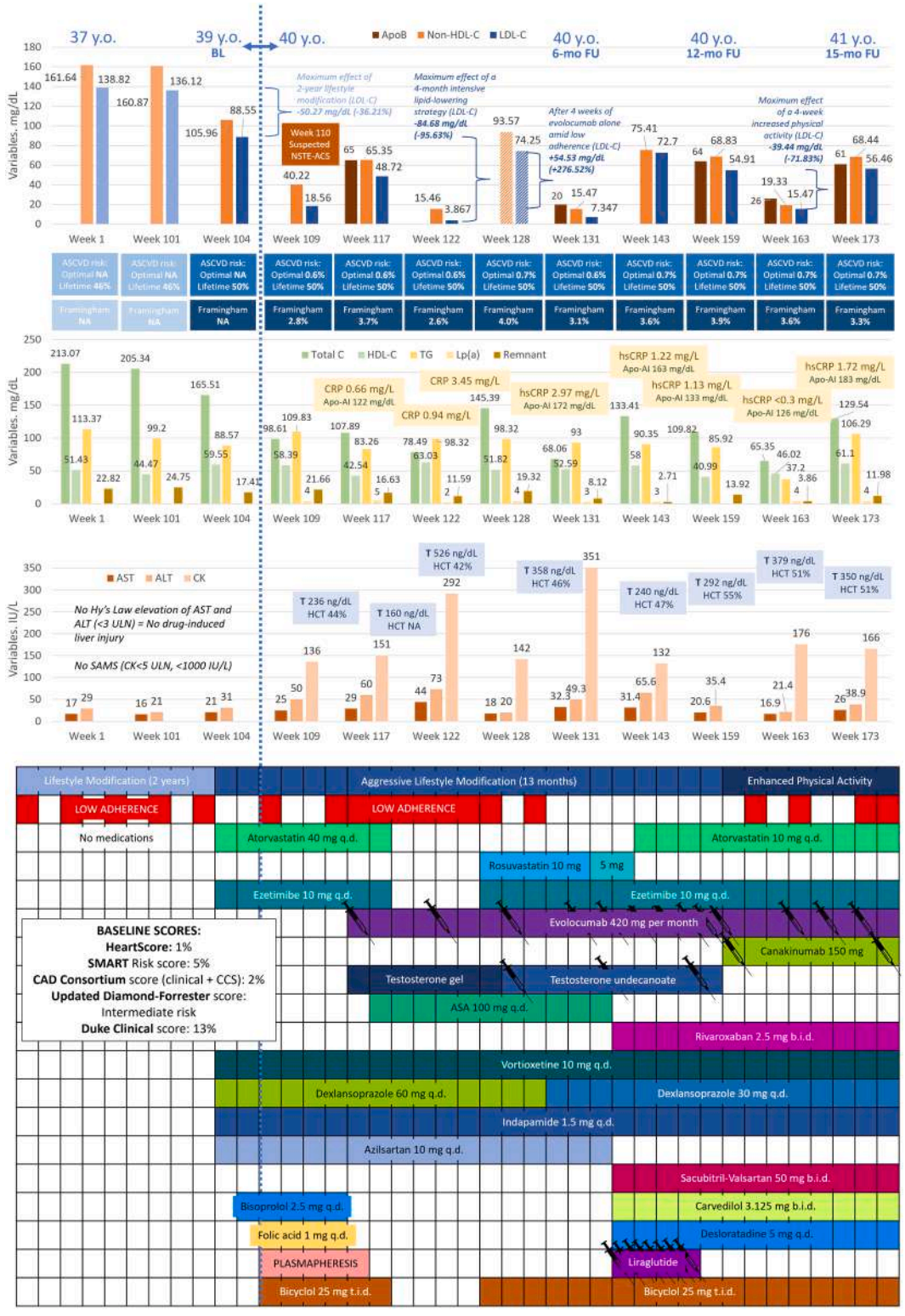

Continued on the next page

probability or deferring the timing of major cardiovascular events, mitigating progression toward heart failure, and potentially exerting a broader "anti-aging" impact on the cardiovascular system through preservation of vascular integrity and functional reserve. Importantly, these benefits must always be balanced against the risks of polypharmacy and off-label interventions; in this case, a structured safety plan and continuous monitoring ensured that no treatment-limiting adverse events occurred, reinforcing the feasibility of such a strategy when guided by vigilant risk-benefit assessment.

CONCLUSIONS

This case illustrates the clinical value of an intensive, multimodal, and phenotype-guided strategy for managing INOCA in a patient with symptomatic MB, nonobstructive but high-risk atherosclerosis, and systemic inflammation. The integration of advanced imaging tools—including CCTA, ML-IRS, and PCAT analysis—with functional and molecular profiling enabled tailored treatment that extended beyond symptom relief to address underlying mechanisms of ischemia and disease progression. Regression of vulnerable plaque features, improvement in myocardial perfusion, and normalization of inflammatory markers collectively translated into substantial clinical benefit and quality-of-life gains. These findings support an individualized preventive approach in selected high-risk INOCA phenotypes, particularly when conventional anatomical thresholds fail to capture dynamic ischemic risk.

STATEMENT OF CONSENT The patient was enrolled in the REALITY Advanced trial (ClinicalTrials.gov Identifier: NCT02440646). Between 2015 and 2021, the Ural State Medical University (Yekaterinburg, Russia) acted as the trial sponsor and provided ethical oversight. In 2021, these responsibilities were transferred to the Central Clinical Hospital of the Russian Academy of Sciences/Scientific and Clinical Center No. 2, Petrovsky National Research Centre of Surgery (Moscow, Russia), which continued oversight until the study was formally terminated in 2022. The patient provided written informed consent for study participation in April 2019 and for scientific dissemination of his clinical data in August 2022. All examinations and treatments were conducted voluntarily within both the private and compulsory medical insurance sectors of the Russian health care system.

ACKNOWLEDGMENTS The authors acknowledge the use of advanced cardiovascular imaging software tools in this study. Primary image analysis was conducted using Autoplaque (Biomedical Imaging Research Institute, Cedars-Sinai Medical Center, Los Angeles, California, USA), which enabled automated quantification of pericoronary adipose tissue (PCAT) and computation of the machine learning ischemia risk score (ML-IRS), forming the core analytic framework of the study. In addition, Autoplaque facilitated semiautomated plaque characterization through virtual histology, including quantification of tissue components (NCP, LD-NCP, and CP), estimation of total and vessel volumes (mm^3), calculation of

FIGURE 6 Continued

This figure summarizes the temporal changes in lipid profile, inflammatory markers, liver/muscle enzymes, testosterone levels, and medication adherence over a 3-year period in a patient with INOCA undergoing personalized preventive therapy. (Top Panel) LDL-C, non-HDL-C, remnant cholesterol, and ApoB levels were substantially reduced over time—from a baseline LDL-C of 138.8 mg/dL and ApoB of 160.87 mg/dL to nadirs of 7.35 mg/dL and 20 mg/dL, respectively—through an escalating strategy involving high-intensity statins (atorvastatin, rosuvastatin), ezetimibe, and PCSK9 inhibition (evolocumab). Remnant cholesterol declined from 24.75 to 0.07 mg/dL. (Middle Panels) High-sensitivity CRP (hsCRP) initially rose to 3.45 mg/L despite lipid-lowering therapy, prompting the introduction of canakinumab (150 mg every 8 weeks), which reduced hsCRP to <0.3 mg/L. ApoA1 levels increased in parallel. Liver and muscle enzymes remained below toxicity thresholds, and no signs of statin-associated muscle symptoms (SAMS) or hepatotoxicity were observed. Testosterone therapy was tailored and subsequently discontinued upon achieving stable endogenous levels. (Bottom Panel) A detailed medication timeline shows phased intensification of therapy, including ARNI (sacubitril/valsartan), rivaroxaban, SGLT2 inhibitor (dapagliflozin), and colchicine. Lifestyle modification periods, physical activity, and phases of low adherence are annotated. Baseline risk scores were low (HeartScore: 1%, SMART: 5%, CAD Consortium: 2%), yet imaging revealed high-risk plaques, justifying the aggressive preventive approach. This comprehensive overview demonstrates the feasibility and biochemical efficacy of multimodal pharmacologic and lifestyle intervention in high-risk INOCA without obstructive CAD. ALT = alanine transaminase; Apo = apolipoprotein; ARNI = angiotensin receptor neprilysin inhibitor; ASCVD = atherosclerotic cardiovascular disease; AST = aspartate transaminase; CAD = coronary artery disease; CK = creatine kinase; CRP = C-reactive protein; HCT = hematocrit; HDL-C = high-density lipoprotein cholesterol; INOCA = ischemia with nonobstructive coronary arteries; LDL-C = low-density lipoprotein cholesterol; NA = not applicable or not available; T = testosterone.

TABLE 1 CCTA-Based Per-Patient Quantitative Machine Learning Analysis of Coronary Arterial Remodeling With Mean Change of Variables (All Regions of Interest in the LM, LAD, LCx, and RCA Arteries) Between Baseline and Follow-Ups

Variables Assessed With CCTA	Between BL and 6-mo FU	Between 6-mo and 12-mo FU	Between BL and 12-mo FU	Between BL and 15-mo FU	Between 6-mo and 15-mo FU	Between 12-mo and 15-mo FU
Quantitative artificial intelligence/machine learning assessment of coronary perivascular fat density/degree of inflammation (measured in HU) per patient[a]						
Mean PCAT, HU, within a 1 mm radius	+15.96 (+19.17%), $P = 0.059$	+4.01 (+5.95%), $P = 0.65$	+19.97 (+23.98%), $P = 0.10$	−2.94 (−3.54%), $P = 0.34$	**+13.02 (+19.34%), $P = 0.02$**[b]	+17.02 (+26.90%), $P = 0.13$
Tissue volume, mm^3	$P = 0.08$	$P = 0.52$	$P = 0.23$	$P = 0.27$	$P = 0.14$	$P = 0.24$
Mean PCAT, HU, within a 3 mm radius	+17.74 (+19.11%), $P = 0.08$	+3.90 (+5.20%), $P = 0.54$	+21.64 (+23.32%), $P = 0.14$	−8.75 (−9.42%), $P = 0.11$	+8.99 (+11.98%), $P = 0.06$	+12.90 (+18.12%), $P = 0.22$
Tissue volume, mm^3	$P = 0.14$	$P = 0.92$	$P = 0.12$	$P = 0.35$	$P = 0.20$	$P = 0.28$
Mean PCAT, HU, within a 11 mm radius	+12.39 (+13.64%), $P = 0.18$	+3.81 (+4.86%), $P = 0.09$	+16.19 (+17.84%), $P = 0.13$	−6.83 (−7.52%), $P = 0.16$	+5.56 (+7.09%), $P = 0.36$	+9.36 (+12.55%), $P = 0.18$
Tissue volume, mm^3	$P = 0.08$	$P = 0.23$	$P = 0.94$	$P = 0.27$	$P = 0.19$	$P = 0.24$
Quantitative artificial intelligence/machine learning measures in coronary arteries per patient[a]						
Tissue volume, mm^3						
NCP	**+84.64 (+42.87%), $P = 0.006$**[b]	+157.56 (+55.86%), $P = 0.08$	−72.92 (−36.94%), $P = 0.23$	−76.31 (−38.65%), $P = 0.45$	−160.95 (−57.06%), $P = 0.21$	−3.38 (−2.72%), $P = 0.94$
LD-NCP	−14.85 (−32.87%), $P = 0.92$	−19.07 (−62.87%), $P = 0.27$	−33.91 (−75.07%), $P = 0.26$	−26.44 (−58.54%), $P = 0.40$	−11.60 (−38.24%), $P = 0.51$	+7.47 (+66.34%), $P = 0.34$
CP	0	0	0	0	0	0
Estimated total	**+84.64 (+42.87%), $P = 0.006$**[b]	+157.56 (+55.86%), $P = 0.08$	−72.92 (−36.94%), $P = 0.23$	−76.31 (−38.65%), $P = 0.45$	−160.95 (−57.06%), $P = 0.21$	−3.38 (−2.72%), $P = 0.94$
Vessel volume, mm^3	+113.50 (+21.84%), $P = 0.30$	−283.55 (−44.79%), $P = 0.058$	−170.05 (−32.72%), $P = 0.18$	−91.31 (−17.57%), $P = 0.60$	−204.81 (−32.35%), $P = 0.30$	+78.73 (+22.52%), $P = 0.42$
NCP burden, %	+9.41 (+25.97%), $P = 0.30$	−9.50 (−20.81%), $P = 0.13$	−0.09 (−0.25%), $P = 0.98$	−7.75 (−21.38%), $P = 0.33$	−17.16 (−37.59%), $P = 0.10$	−7.66 (−21.19%), $P = 0.11$
LD-NCP burden, %	−2.67 (−33.50%), $P = 0.15$	−1.67 (−31.47%), $P = 0.39$	−4.34 (−54.43%), $P = 0.16$	−3.42 (−42.86%), $P = 0.23$	−0.75 (−14.07%), $P = 0.59$	+0.92 (+25.39%), $P = 0.30$
Max diameter stenosis, %	+12.61 (+33.02%), $P = 0.38$	−25.34 (−49.89%), $P = 0.12$	**−12.73 (−33.34%), $P = 0.01$**[b]	−12.51 (−32.76%), $P = 0.46$	−25.12 (−49.45%), $P = 0.08$	+0.23 (+0.89%), $P = 0.99$
Max area stenosis, %	+13.66 (+22.17%), $P = 0.34$	−30.43 (−40.43%), $P = 0.13$	**−16.77 (−27.22%), $P = 0.004$**[b]	−16.33 (−26.52%), $P = 0.48$	−29.99 (−39.85%), $P = 0.13$	+0.44 (+0.97%), $P = 0.98$
Plaque length, mm	+5.98 (+21.53%), $P = 0.34$	−11.88 (−35.21%), $P = 0.09$	−5.90 (−21.26%), $P = 0.25$	+12.55 (+45.20%), $P = 0.39$	+6.57 (+19.48%), $P = 0.67$	+18.45 (+84.42%), $P = 0.19$
CDD, %	−5.01 (−22.23%), $P = 0.81$	−12.44 (−70.92%), $P = 0.41$	−17.45 (−77.38%), $P = 0.10$	−1.13 (−5.01%), $P = 0.94$	+3.88 (+22.14%), $P = 0.73$	+16.32 (+320%), $P = 0.17$
MLD, mm	−0.55 (−20.81%), $P = 0.33$	+0.83 (+39.65%), $P = 0.25$	+0.28 (+10.59%), $P = 0.47$	−0.37 (−14.12%), $P = 0.39$	+0.18 (+8.44%), $P = 0.63$	−0.65 (−22.35%), $P = 0.10$
MLA, mm^2	−1.65 (−29.59%), $P = 0.33$	+2.88 (+73.43%), $P = 0.25$	+1.23 (+22.12%), $P = 0.45$	−1.51 (−2.74%), $P = 0.39$	+0.14 (+3.57%), $P = 0.90$	−2.74 (−40.28%), $P = 0.11$
Virtual histology, volume						
Fibrous, mm^3 (%)	**+70.97 (+229.91%), $P = 0.02$**[b]	**−59.03 (-57.97%), $P = 0.045$**[b]	+11.93 (+38.66%), $P = 0.60$	+21.27 (+68.90%), $P = 0.17$	−49.70 (−48.81%), $P = 0.11$	+9.33 (+21.81%), $P = 0.70$
Fibrous fatty, mm^3 (%)	+28.53 (+23.51%), $P = 0.08$	−79.43 (−52.99%), $P = 0.18$	−50.90 (−41.94%), $P = 0.30$	−71.10 (−58.58%), $P = 0.30$	−99.63 (−66.47%), $P = 0.22$	−20.20 (−28.67%), $P = 0.43$
Necrotic core, mm^3 (%)	−11.87 (−29.01%), $P = 0.19$	−17.87 (−61.54%), $P = 0.30$	−29.73 (−72.70%), $P = 0.25$	−24.00 (−58.68%), $P = 0.36$	−12.13 (−41.79%), $P = 0.49$	+5.73 (+51.34%), $P = 0.30$
Dense calcium, mm^3 (%)	0 (0)	0 (0)	0 (0)	0	0	0
AI/ML ischemia score	−0.026 (−9.62%), $P = 0.83$	−0.178 (−71.83%), $P = 0.28$	−0.204 (−74.54%), $P = 0.16$	−0.132 (−48.11%), $P = 0.37$	−0.105 (−42.59%), $P = 0.54$	+0.072 (+103.83%), $P = 0.11$

[a]Data were analyzed by the team of Damini Dey (Biomedical Imaging Research Institute, Department of Biomedical Sciences, Cedars Sinai Medical Center, Los Angeles, California, USA), and then selectively validated by Dr Nicola Gaibazzi (Azienda Ospedaliero-Universitaria di Parma, Parma, Italy). [b]Statistically significant findings (P values derived from 2-tailed paired t tests; statistical significance defined as $P < 0.05$). Tissue volume remained stable across timepoints (nonsignificant P values), verifying that compositional and inflammatory changes reflect true remodeling within anatomically comparable regions. CP = 0 at all timepoints, consistent with a noncalcified atherosclerotic phenotype. The mean change for tissue volume is not provided; a P value >0.05 proves the absence of the difference between the examined ROI between the baseline and follow-ups (therefore, the sites are comparable).

AI = artificial intelligence; AS = percent area stenosis; BL = baseline (at week 106 of the outpatient supervision); CCTA = coronary computed tomography angiography; CDD = contrast density difference; CP = calcified plaque; DS = percent diameter stenosis; FU = follow-up; LAD = left anterior descending artery; LCx = left circumflex artery; LD-NCP = low-density noncalcified plaque; LM = left main artery; max = maximum; ML = machine learning; MLD = minimal lumen diameter; NCP = noncalcified plaque; PB = plaque burden; PCAT = pericoronary adipose tissue; RCA = right coronary artery; ROI = region of interest.

plaque burden and low-density burden (%), maximum diameter and area stenosis (%), plaque length (mm), calcified dense deposit (CDD, %), minimal lumen diameter (MLD, mm), and minimal lumen area (MLA, mm^2). In contrast, Medis Suite (Medis Medical Imaging Systems BV, Leiden, the Netherlands) and CAAS Workstation (Pie Medical Imaging BV, Maastricht, the Netherlands) were employed for complementary purposes, including anatomical localization, 3D coronary artery reconstruction, and plaque composition assessment. We extend our sincere gratitude to the team at HeartFlow Inc (Redwood City, California, USA) for their expert-level assistance in imaging software analysis, particularly acknowledging the personal involvement of Mr Tim Fonte, vice president of customer success. The authors used generative artificial intelligence tools to assist with language editing and summarization during the preparation of this manuscript. These tools were used in a supportive role only. All scientific interpretations, conclusions, and final wording are the sole responsibility of the authors.

The multimodal diagnostic and therapeutic workup of the patient was financially supported by an unrestricted grant from the Ural Regional Construction Company/UralRegionStroy (Yekaterinburg, Russia). We express our sincere gratitude to Dr Irina Shurupova, MD (PET Center, Bakulev National Medical Research Center for Cardiovascular Surgery, Moscow, Russia), and Dr Maksim Kashtanov, MD, PhD (Department of Interventional Radiology, Center for Heart and Vessels, First Regional Clinical Hospital, Yekaterinburg, Russia), for their valuable contributions in the interpretation of nuclear imaging data and expert advice in interventional radiology, respectively.

Dr Kharlamov gratefully acknowledges the support received from the FP7-IIF Marie Curie Individual Fellowship program of the European Commission (2011-2013) for the DREAM project (Development of Bioresorbable Scaffolds and Nanotechnologies for Reversal of Atherosclerosis; Grant No. 329728 under FP7-PEOPLE-2012-IIF), led by Prof Patrick Serruys, MD, PhD (Erasmus MC, Rotterdam, the Netherlands; Imperial College, London, UK; University of Galway, Galway, Ireland). The project greatly inspired the investigators of the REALITY Advanced trial (NCT02440646) for several years, until its suspension in March 2022 and formal termination in August 2022.

FUNDING SUPPORT AND AUTHOR DISCLOSURES

The authors have reported that they have no relationships relevant to the contents of this paper to disclose.

ADDRESS FOR CORRESPONDENCE: Dr Alexander Kharlamov, DHRF, Keurenplein 41, Box G9950, Amsterdam 1069CD, the Netherlands. E-mail: drkharlamov@icloud.com.

REFERENCES

1. Matta A, Nader V, Canitrot R, et al. Myocardial bridging is significantly associated to myocardial infarction with non-obstructive coronary arteries. *Eur Heart J Acute Cardiovasc Care*. 2022;11(6):501-507. https://doi.org/10.1093/ehjacc/zuac047

2. Guerra E, Bergamaschi L, Tuttolomondo D, Pizzi C, Sartorio D, Gaibazzi N. Contrast stress echocardiography findings in myocardial bridging compared to normal coronary course, with and without coronary artery disease. *J Am Soc Echocardiogr*. 2023;36(10):1092-1099. https://doi.org/10.1016/j.echo.2023.06.008

3. Padro T, Manfrini O, Bugiardini R, et al. ESC working group on coronary pathophysiology and microcirculation position paper on coronary microvascular dysfunction in cardiovascular disease. *Cardiovasc Res*. 2020;116(4):741-755. https://doi.org/10.1093/cvr/cvaa003

4. Arbab-Zadeh A, Fuster V. The risk continuum of atherosclerosis and its implications for defining CHD by coronary angiography. *J Am Coll Cardiol*. 2016;68(22):2467-2478. https://doi.org/10.1016/j.jacc.2016.08.069

5. Lee SE, Sung JM, Andreini D, et al. Differences in progression to obstructive lesions per high-risk plaque features and plaque volumes with CCTA. *JACC Cardiovasc Imaging*. 2020;13(6):1409-1417. https://doi.org/10.1016/j.jcmg.2019.09.011

6. Lee SE, Chang HJ, Sung JM, et al. Effects of statins on coronary atherosclerotic plaques: the PARADIGM study. *JACC Cardiovasc Imaging*. 2018;11(10):1475-1484. https://doi.org/10.1016/j.jcmg.2018.04.015

7. Ference BA, Ginsberg HN, Graham I, et al. Low-density lipoproteins cause atherosclerotic cardiovascular disease. 1. Evidence from genetic, epidemiologic, and clinical studies. A consensus statement from the European Atherosclerosis Society consensus panel. *Eur Heart J*. 2017;38(32):2459-2472.

8. Guedeney P, Claessen BE, Kalkman DN, et al. Residual inflammatory risk in patients with low LDL cholesterol levels undergoing percutaneous coronary intervention. *J Am Coll Cardiol*. 2019;73(19):2401-2409. https://doi.org/10.1016/j.jacc.2019.01.077

9. Reynolds HR, Diaz A, Cyr DD, et al. Ischemia with nonobstructive coronary arteries: insights from the ISCHEMIA trial. *JACC Cardiovasc Imaging*. 2022;15(12):2223-2236. https://doi.org/10.1016/j.jcmg.2022.06.015

10. Kunadian V, Chieffo A, Camici PG, et al. An EAPCI expert consensus document on ischaemia with non-obstructive coronary arteries. *Eur Heart J*.

2020;41(37):3504–3520. https://doi.org/10.1093/eurheartj/ehaa503

11. Fernández-Friera L, Fuster V, López-Melgar B, et al. Normal LDL-cholesterol levels are associated with subclinical atherosclerosis in the absence of risk factors. *J Am Coll Cardiol*. 2017;70(24):2979–2991. https://doi.org/10.1016/j.jacc.2017.10.024

12. Ference BA, Graham I, Tokgozoglu L, Catapano AL. Impact of lipids on cardiovascular health: JACC health promotion series. *J Am Coll Cardiol*. 2018;72(10):1141–1156. https://doi.org/10.1016/j.jacc.2018.06.046

13. Kwan AC, McElhinney PA, Tamarappoo BK, et al. Prediction of revascularization by coronary CT angiography using a machine learning ischemia risk score. *Eur Radiol*. 2021;31(3):1227–1235. https://doi.org/10.1007/s00330-020-07142-8

14. Kharlamov A, Lamberts M. Digital medicine: the next big leap advancing cardiovascular science. *BMC Cardiovasc Disord*. 2023;23(1):30. https://doi.org/10.1186/s12872-022-02971-5

KEY WORDS advanced cardiovascular imaging, chronic coronary syndrome, ischemia, machine learning, microvascular dysfunction, myocardial bridge, nonobstructive coronary atherosclerosis

APPENDIX For supplemental materials, please see the online version of this paper.